Single-Photon-Induced Post-Ionization to Boost Ion Yields in MALDI Mass Spectrometry Imaging

Christoph Bookmeyer
University of Münster https://orcid.org/0000-0002-3479-3841
Ulrich Röhling
University of Münster
Klaus Dreisewerd
University of Münster https://orcid.org/0000-0002-7619-808X
Jens Soltwisch (jenssol@uni-muenster.de)
University of Münster https://orcid.org/0000-0002-0258-1561

Article

Keywords: MALDI-MSI, single-photon photoionization, laser-based postionization

Posted Date: September 29th, 2021

DOI: https://doi.org/10.21203/rs.3.rs-923767/v1

Abstract

Matrix-assisted laser desorption/ionization mass spectrometry imaging (MALDI-MSI) is a rapidly growing method in many fields of the life sciences. For many analyte classes, however, its sensitivity is limited due to poor ionization efficiencies. To mitigate this problem, we here introduce a novel and cost-effective postionization scheme at high repetition rates based on the interplay of single-photon photoionization and subsequent charge transfer reactions. Importantly, the fine vacuum conditions of a dual ion-funnel ion source effectively thermalize the evolving MALDI plume and enable ample gas-phase reactions as well as the addition of chemical dopants that crucially support chemical ionization. Supported by acetone dopant, $[M + H]^+/[M-H]^-$ signals of numerous glycerophospho-, sphingo-, and further lipids, registered from mammal brain and kidney sections, were boosted by up to three orders of magnitude, similar to results obtained with laser-based postionization (MALDI-2). Experiments utilizing deuterated matrix and dopant, however, indicate complex ionization pathways different from MALDI2.

Introduction

Mass spectrometry imaging (MSI) is a label-free technique that is increasingly used to visualize the spatial distribution of numerous classes of biomolecules, such as lipids, numerous further secondary metabolites, and tryptic peptides in biological samples like thin tissue Sect. [1–4] The most widely used 'soft' desorption/ionization technique in MSI applications is matrix-assisted laser desorption ionization (MALDI). [5] Most commercially available MALDI-MSI instruments now provide a lateral resolution in the 5–20 μm range and recent methodological developments demonstrated the potential of MALDI-MSI with a pixel size of about 1 μm and smaller. [6,7] A notable limitation of the method, especially in high-resolution applications, where only minute amounts of material are available per pixel, are low MALDI ion yields. It is estimated that for numerous analyte classes less than one in a million of the ejected molecules are also concomitantly ionized. [8] In addition, molecules with high ion affinities can cause ion suppression effects by abstracting charges from other compounds during the MALDI process. A common example for ion suppression is presented by phosphatidylcholines (PC), which in the positive ion mode notoriously hamper the detection of the many other lipid classes present in complex tissues. [9,10]

To meet these challenges, various postionization (PI) techniques have been developed, fostering the analytical depths of an experiment. [3,4] In this regard, a number of methods based on charge distribution reactions have been introduced recently that enable increased ionization efficiencies for a much broader range of analytes. Because these methods rely on gas-phase reactions between neutrally desorbed analyte molecules and separately ionized charge donors, they require elevated pressure conditions, typically in the range of a few mbar or even atmospheric pressure. Most prominently, a method coined MALDI-2 utilizes an additional pulsed UV laser to irradiate the expanding MALDI plume to effectively postionize neutral matrix molecules in a two-photon ionization process under fine vacuum conditions. [11,12] The resulting confinement of the expanding MALDI plume leads to the formation of a temporary reaction vessel and a cascade of secondary MALDI-like ionization reactions. A consequential boost of the

ion signal intensities by up to 2–3 orders of magnitude has been reported for numerous analyte classes including lipids, glycans, a range of further secondary metabolites, and pharmaceuticals. [11–18] In an alternative approach, molecules that are neutrally desorbed during a MALDI-MSI experiment at atmospheric pressure are collected by a stream of gas and allowed to react with ions separately produced in a cold plasma. [19] Similar to MALDI2, signals for a number of lipid classes, which notoriously suffer from ion suppression effects, are increased sizably.

Next to utilizing charge distribution reactions, another means for ionizing gaseous molecules is by use of high-energetic vacuum ultraviolet (VUV) light. Here, photon energies of ~ 10 eV enable efficient single-photon ionization (SPI) of a broad range of biomolecules due to an optimal trade-off between low fragmentation rates and high ionization yields. The method, therefore, has been envisioned as “universal and soft”. [20] In practice, at least a moderate degree of fragmentation is often observed upon direct SPI even for various classes of small molecules, [21] and reported analyte ions rarely exceed *m/z*-values larger than 500. [22]

Whereas with direct SPI the ionization commonly takes place in high vacuum, e.g., to avoid unwanted side reactions with other gas components, arguably the most important application of SPI is the analysis of volatile organic compounds (VOC) within atmospheric pressure photoionization (APPI) that utilizes such gas-phase reactions to increase analyte ion yields – e.g., for less polar compounds. [23] Herein, neutral gaseous molecules (e.g., less polar compounds) are produced by a heated nebulizer. Most commonly, dopant vapor (e.g., of acetone or toluene) is added to foster the desired charge transfer reactions. [23] Another SPI variant, where the ionization takes place in a fine vacuum environment of a few mbar of N_2, is referred to as low-pressure photoionization (LPPI). The main advantages of LPPI compared to APPI are reduced side reactions with atmospheric oxygen or nitric compounds and lower degrees of fragmentation due to adiabatic cooling scenarios. [24] Moreover, at a few mbar of N_2, dopant vapor can straightforwardly be added. As an example of LPPI-MS of VOC and semi (s)VOC using Kr discharge lamps in a dual ion funnel–dual MALDI/ESI source, we previously registered several hundred VOC from exhaled human breath and thousands of (s)VOC from coffee roasts using a simple capillary-based sample and dopant introduction system. [25]

Kr discharge lamps emit light with main emission lines at 117 and 124 nm (corresponding to photon energies of 10.6 and 10.0 eV). In comparison to lasers, the photon density is considerably lower, and the emission is typically continuous, incoherent, and challenging to focus. As these lamps are much easier to handle and are more cost-effective than lasers, however, they comprise suitable light sources for APPI. [23]

Laser desorption has been successfully combined with laser-based SPI for postionization of small molecules, e.g., to detect metabolites from bacterial and yeast biofilms. [26] SPI has also been combined with MALDI in a high-vacuum source to postionize amino acid standards. [27]

Here we report the first application of a pulsed VUV lamp module for efficient PI of a broad range of lipid analytes in a fine-vacuum MALDIMS imaging setting. A set of fundamental studies performed using deuterated matrix and dopants to analyze lipid standards revealed a high degree of chemical interaction within the confined plume. To account for the fundamental mechanistic differences to those reported for MALDI-2 we will refer to the method in the following as Single-Photon Induced Chemical Ionization (SPICI). We demonstrate the analytical capabilities of MALDI-SPICI-MSI at the examples of mouse brain and kidney sections and of pig brain homogenate analyzed at 16–20 µm pixel sizes. Here, signal intensities of numerous glycerophospho- and (glyco-)sphingolipids, as well as further compounds, are boosted by up to several orders of magnitude.

Results And Discussion

The general layout of our PI source is sketched in Fig. 1, and, in more technical detail presented in Figure S-1 of the online Supplementary Information (SI). In brief, the matrix-coated sample is irradiated by a series of ns-long UV laser pulses of 349 nm wavelength on a pixel-by-pixel basis, analogous to a classical MALDI-MSI experiment. The ejected plume of material is irradiated by three RF-Krypton discharge lamps operated at 13.560 MHz. Lamps are driven by custom-made electronics operated in pulsed mode with an adjustable pulse width from a minimum of 70 µs (ignition time; see Fig. 2b) to continuous operation. In pulsed mode, the emission bursts of radiation are synchronized with the MALDI laser. The ion source is operated at fine vacuum conditions of about 10 mbar of N_2 and dopant vapor (e.g., acetone) is introduced via a capillary system. Under these conditions, the mean free path within the background gas is on the order of a few microns, and ions generated by the primary SPI process are subject to ample collisions with other neutral and charged molecules, such as matrix, analytes, dopant gas, and residual water vapor, which together allows for numerous charge transfer reactions. Further instrumental detail as also data acquisition and evaluation workflows are provided in the online methods.

Optimizing experimental parameters

To characterize and optimize the performance characteristics of our PI module, we utilized thin sections of matrix-coated pig brain homogenate prepared as described earlier. [11] 2,5Dihydroxyacetophone (DHAP) was used as the MALDI matrix in all reported experiments. Different MALDI matrices like 2,5-dihydroxybenzoic acid (DHB), a few polycyclic aromatic hydrocarbons (PAH), and norharmane were also tested. Compared to DHAP, the latter generally resulted in lower PI yields and higher background signal intensities. The laser pulse energy for the initial MALDI event was carefully adjusted for optimal MALDI performance with regard to ion yields of intact lipid species for MALDI and MALDI-SPICI, respectively. Similar to observations made for MALDI2, SPICI requires considerably increased laser pulse energies for optimal performance as compared to classical MALDI. Even though the employed laser system and the VUV-lamp module allow for the use of pulse repetition rates as high as 5 kHz, the acquisition speed of the Q Exactive Plus Orbitrap limits the amenable scanning rates. An optimum of the overall signal intensities with a frequency of 300 Hz for laser and synchronized pulsed VUV bursts was identified and used as a

setting for the following experiments. The absolute pressure inside the ion source in a range from 8–12 mbar had only a minor influence on the general quality of mass spectra (Fig. 2f,g). Similarly, the absolute values of the extraction voltage U_{xtr} did not show to have a major effect on the ion signal intensity over a range from 330 to 510 V (Fig. 2f,g). However, to obtain a reproducible data quality during the partially hours long MALDI-SPICI-MSI runs, it was crucial to realize stable conditions for the gas phase (buffer gas pressure and dopant) and the electric field.

Two mass spectra, recorded from pig brain homogenate with and without SPICI postionization, are displayed in Fig. 2a. The MALDI-MS measurement generated a total ion count (TIC) of ~ 10^4 counts per second (cps) for the *m/z* range from 450 to 1600 and upon averaging over 300 pixels. In the central 'phospholipid region' between about *m/z* 700 to 850, mainly Na^+- and K^+-adducts of major PCs are registered, in accordance with general experience for this tissue type. [11]

The MALDI-SPICI mass spectrum recorded over the same number of pixels reflects a substantially enhanced chemical coverage and a TIC that is increased by a factor of ~ 2–3. Next to different lipoforms of sphingolipids such as monohexosylceramides (HexCer), ceramides (Cer), and phosphatidylethanolamine ceramides (PECer), numerous species of phospholipids other than PC (e.g., different lipoforms of phosphatidylethanolamines (PE), phosphatidylserines (PS), and various plasmalogens) were detected with sizable signal intensities. All assignments are based on accurate mass, LIPID MAPS® data bank entries, [28] and comparison with literature data [16,29–32] (*cf.* Table S-1 for *m/z* values and reference data). In general, MALDI-SPICI spectra largely resemble spectra recorded with laser-based MALDI-2. As with MALDI-2, intact protonated $[M + H]^+$ species were the main beneficiaries of the SPI-induced PI processes, whereas the signals of alkali metal adducts were not amplified. [11,33] Overall, a total of 200 different lipid species was tentatively assigned based on accurate mass from pig brain homogenate samples in the *m/z* range from 450 to 1600 (Table S-1, SI).

As an example, the extracted ion signal intensities for all tentatively assigned protonated phosphatidylethanolamine (PE) species (including PE plasmalogens) are plotted in Fig. 2c. In comparison to quantitative LC-ESI-MS measurements of pig brain extract, [29] all PE lipoforms are recorded with relative normalized signal intensities that deviate by less than 20 % from the LC-MS data. This margin lies well within the range of the expected biological variation and, hence, the result could indicate a notable potential of the method for semi-quantitative analyses. Next to neutral molecules related to the MALDI event, signal intensities of chemical noise – most prominently several polysiloxane- and plasticizer-derived signals – are sizably enhanced by SPICI (Figure S-2, SI). Most likely, these originate from contaminations of the laboratory atmosphere which are constantly introduced into the ion source, e.g., during sample loading.

The effectiveness of SPICI postionization depends on a few basic experimental premises regarding the VUV-irradiation and the introduction of a dopant that need to be adjusted for optimal results, including partial reduction of unwanted background signals.

Optimizing VUV-irradiation – A pulsed operation of the Kr lamps that is carefully synchronized with the MALDI-process sizably improves the stability of ion signals and the quality of the acquired mass spectra. By optimizing the pulse duration, signal intensities of chemical noise are substantially reduced. While polysiloxane signal intensities steadily increase with the duration of the electronic excitation pulse τ_{VUV} that produces the VUV light, lipid ion counts were found to first increase rapidly with the onset of VUV radiation before a plateau is reached for $\tau_{VUV} \geq 300$ µs (Fig. 2b). This results in an optimized signal-to-noise ratio (s/n-ratio) at a pulse width between 300 and 400 µs. To ensure a steady measurement inside the plateau region, all experiments described in the following were conducted with $\tau_{VUV} = 350$ µs, resulting in an effective length of the VUV light pulse after ignition of 280 µs. The delay between the MALDI laser pulse and the start of the VUV burst was adjusted to different values relative to the laser shot. Somewhat surprising, the delay did not show to be relevant with regard to the efficiency of the SPICI process. Peculiarly, in a time window of approximately − 100 µs to + 100 µs with regard to the MALDI event, the overall signal decreased by about 20 % at most. These results stand in contrast to laser-based MALDI-2, where neutrally ablated matrix molecules are directly photoionized around 10 µs after the MALDI event and point to significant differences in the ionization process. In a first attempt to describe the underlying mechanism, it could be rationalized that relatively stable dopant ions are produced via SPI. After the initial material ejection, the MALDI-plume diffuses into the background gas and charges are transferred from the charged dopant to analyte molecules. The pulse duration of the employed VUV bursts can be used to control the concentration of charged dopant inside the ion source and data suggest that optimal concentrations are reached for a pulse duration of around 300–350 µs (Fig. 2b). At the same time, chemical noise is continuously produced during VUV irradiation by LPPI in the gas phase and can be reduced by utilizing short VUV pulses. Speculatively, the observed dip in signal intensity for small delays between VUVburst and laser pulse may be explained by local recombination reactions between molecular ions and photoelectrons produced by SPI.

Optimizing dopant parameters - High yields for SPICI postionization crucially depend on the use of a suitable dopant at carefully controlled conditions. In this study, primarily acetone was used. Measurements with toluene, anisol, and chlorobenzene as dopants resulted in the detection of similar $[M + H]^+$ species but with lower signal intensities and higher background intensities. Figure 2d illustrates the effect of dopant on the signal registered at *m/z* 538.52, which is tentatively assigned to $[Cer(d36:1) + H]^+$ and exemplary chosen as one of the numerous analyte-derived ion signals benefitting from SPICI. The signal intensities drastically increase with increasing partial pressure for the dopant and reach a plateau at a value of 0.16 mbar. Meanwhile, polysiloxane-derived background signals were crucially reduced when acetone dopant was introduced into the source with partial pressures in excess of ~ 0.10 mbar. This unexpected effect is demonstrated in the example of the siloxane octamer signal at *m/z* 593.2 (Figs. <link rid="fig2">2</link>e, S-2). Although reduced by the use of pulsed irradiation and optimized partial pressure of the dopant, chemical noise remained the dominating signals in the lower mass range in the positive ion mode (+). Therefore, all presented (+)-MALDI-SPICI-MSI measurements are recorded in a mass range of above *m/z* 450. The following data was furthermore recorded with optimized conditions of P_{total} = 8.5 mbar, $P_{partial}$(acetone) = 0.16 mbar, U_{xtr} = 400 V, and U_t = 400 V.

MALDI-SPICI-MSI

Making use of the optimized parameter settings, we next explored the potential of our method for MALDI-MS imaging of mouse brain sections. Selected ion images, as plotted in Fig. 3, again visualize a major increase in the analytic depth between MALDI-SPICI and conventional MALDI. The total measurement time in this experiment, recorded with a mass resolving power of 140,000 (at *m/z* 200) was 42 hours. The ion images are presented without normalization and, thus, reflect high robustness in the signal generation over such an extended period of time. With SPICI postionization, the analytical capabilities are extended substantially, allowing for a more detailed characterization of the distribution of numerous lipid classes in different tissue regions like the white matter or the molecular layer. The benefit of the high mass resolving power that is provided by the Orbitrap mass analyzer is demonstrated exemplary in the zoom-in of a narrow mass window between *m/z* 774.4 and 774.8 (Fig. 3p). Within a mass window of < 0.2 Da alone, six different ion species are registered with acceptable separation. The (partly) differential distribution of these compounds in the brain is shown in panels g-m of Fig. 3. Overall, based on accurate mass, about 250 different lipid species were registered in the mouse brain using MALDI-SPICI-MSI (Table S-1, SI).

As a second example, selected ion images recorded from a mouse kidney section are displayed in Figure S-3 (SI). Exemplarily, we tentatively assigned protonated signals of Cer(d42:1), PS(38:4) and Cardiolipin (CL)(76:6) in the cortex, Hex_2Cer(d32:1) in the medulla, LPE(18:1) in the Calyx/Pelvis; a number of not yet identified signals with *m/z* > 1,600 were moreover found in vessels.

The high signal intensities that are obtained for many analyte species allow for efficient tandem MS analyses for structure elucidation. To demonstrate this important feature, we made use of data-dependent acquisition MS/MS (DDA-MS/MS) [31] to measure a mouse brain section that was adjacent to the tissue section used to produce the MS^1 data of Fig. 3. In this Top4 experiment, one full scan pixel is sequentially followed on the next four pixels by four automated MS/MS experiments of the highest signals with a dynamic exclusion time of 10 s per distinct *m/z* value. Figure 4a depicts average MS/MS spectra acquired for three exemplary *m/z* values. The MS images of the respective signal intensity distribution in the full scan mass spectra are shown in Fig. 4b. In total, 40 lipid species could be identified by the DDA experiments and serve as additional confirmation of the tentative assignments for mouse brain data based on accurate mass as listed in Table S1 (SI).

Negative ion mode

A set of mass spectra and ion images was also recorded from DHAP-coated tissue sections in the negative ion mode. Notably, similar settings for the operation of the pulsed RF lamp and acetone dopant supply as in the positive ion mode provided optimal MS results; the settings optimized with pig brain homogenate as a standard sample were: P_{total} = 8.5 mbar, $P_{partial}$(acetone) = 0.2 mbar, U_{xtr} = 360 V, U_{target} = 400 V, τ_{VUV} = 350 µs. Again, negative ion mode MALDI-SPICI-MS data resemble those acquired with laser-based MALDI2 with regard to both the boosted chemical coverage/signal strength of, e.g.,

numerous glycerophospho- and sphingolipids as well as to the type of predominantly recorded ions (i.e., $[M - H]^-$; Figure S-4, SI). [11,16]

Notably, in contrast to the positive ion mode, background substances were ionized with only low intensity in the negative ion mode and were suppressed to an almost negligible intensity when pulsed operation and a controlled partial dopant pressure with $P_{partial}$(acetone) > 0.1 mbar were applied. Consequently, negative ion mode MALDI-SPICI-MS can more readily be used to cover smaller metabolites down to about *m/z* 200 depending on the employed MALDI matrix. The less effective ionization of compounds in the surrounding gas phase – background signals – is in accordance with the selected ionization efficiencies reported in the literature for APPI-MS in the negative mode. [23] In MALDI-PI, however, the high coverage of the lipid profile in the negative ion mode stands in contrast to the selective ionization pathways described for negative ion mode APPI-MS and is an indication for different ionization mechanisms in APPI and SPICI.

A mouse brain section measured with MALDI-SPICI-MSI in the negative ion mode is shown in Figure S-5 (SI). A broad range of detected signals could be tentatively assigned as deprotonated species of cerebral lipids of numerous lipid classes in a wide mass range for example from cyclic lyso-glycerophospholipids (GPL) like $[cLPA(16:0) - H]^-$ (*m/z* 391.23) up to high masses of an intact monosialotetrahexosylganglioside $[GM1(d36:1) - H]^-$ (*m/z* 1544.87). Similar to the positive ion mode, the majority of depicted ion signals was obtained only upon PI. Due to the measuring principle of the employed mass spectrometer, ion signals with high intensity measured for volatile molecules like free fatty acids in the mass range of *m/z* < 320 (see Figure S-6, SI) can compromise the signal intensities for higher mass compounds. For that reason, the MALDI-SPICI-MSI experiments shown in this work were recorded in the mass range of *m/z* > 320. In total, based on accurate mass, about 270 different lipid species were registered from the brain tissue in the *m/z* range from 320 to 1600 in the negative ion mode. Measuring brain homogenate within a Top4-DDA-MS/MS MALDI-SPICI experiment, a total number of 56 lipid annotations could be structurally confirmed (*c.f.* Table S1, SI).

Ionization Mechanism

None of the investigated tissues showed any visible degradation after illumination with the undirected VUV light and no chemical alterations of the lipids are apparent from the MS-images recorded over long periods of time. Furthermore, no desorption without ablation laser impact was monitored, and no carry-over between pixels is observable in the MS images. Based on these observations, we reason that the VUV-induced postionization takes place only at the interplay of the laser plume, VUV pulse, and dopant altogether. To gain further insights into the ionization mechanism as well as into possible fragmentation pathways, we conducted a series of experiments with phospholipid standards, namely PS(16:0/18:1) and PC(16:0/18:1), by use of deuterated DHAP matrix, acetone-d_6, and D_2O, respectively. Lipid standard solutions were sprayed on histological glass slides and covered with matrix by sublimation. MALDI-SPICI spectra were generated by averaging over 60 pixels (1 min) per parameter set. Details of the sample

preparation, the synthesis of deuterated DHAP, and further experimental details are described in the online methods.

The use of perdeuterated acetone as a dopant resulted in no visible changes in the mass spectra as compared to regular acetone. In particular, no auto-deuteronation of the dopant and thus no deuteronation of the analytes was observed; acetone was recorded solely as protonated species (Figure S-7, SI), in line with results from APPI experiments. [34]

Using deuterated DHAP matrix and regular acetone as the dopant, the recorded mass spectra revealed differences to those obtained with regular matrix. Expectedly, in the MALDI-only experiment, an isotope distribution with different degrees of hydrogen-deuterium-exchange (HDX) of the accessible hydrogen atoms is visible with the signal for $[PS(34:1)d_2 + D]^+$ forming the base peak in the mass spectrum (Fig. 5a1). If the VUV lamps are switched on, the picture changes entirely (Fig. 5a2). No HDX is visible in the spectra and the $[M + H]^+$ signal of PS(34:1) forms the base peak with the expected isotopic pattern. We attribute this finding to a high degree of chemical interaction in the confined plume between photo-activated acetone, matrix, and analyte ions and molecules. This appears to lead to complete deuterium-hydrogen-exchange (DHX) towards the large reservoir of acetone within the overall SPICI process.

Using D_2O, which was introduced into the ion source with $P_{partial} \leq 0.04$ mbar (see online methods), moderate levels of HDX in the gas phase resulted in $[PS(34:1)d_1 + D]^+$ as the base peak of an isotopic distribution pattern in the mass spectrum for regular MALDI experiments (Fig. 5b1). This result is generally in line with MALDI-MS data published by Kostyukevich *et al*. These authors reported different degrees of HDX from GPL after the introduction of D_2O vapor in the fine vacuum atmosphere of a dual ion funnel device similar to the one used in our study with, e.g., up to four labile hydrogen atoms of PS. [35] Upon use of SPICI postionization, a higher degree of HDX was observed, with $[PS(34:1)d_3 + D]^+$ now forming the base peak (Fig. 5b2).

Together, these findings suggest that the decisive proton (or deuteron) donor in the MALDI-SPICI ionization event is not the MALDI matrix, but rather ubiquitous protic molecules like residual H_2O in the gas phase appear to be pivotal contributors. Highly concentrated (acetone) dopant molecules occur to mediate the proton transfer after excitation by the VUV pulse. For acetone, this happens presumably by the formation of an intermediate state of a formally protonated carboxylic group. The suggested main gas-phase ionization step with protonated and deuteronated acetone, respectively, is shown in Fig. 5d. It should be emphasized that the hydrogen atoms of the acetone methyl groups do not directly take part in the proton transfer reaction.

The results from analogous deuteration experiments with the PC(34:1) standard are summarized in Figure S-8 (SI). PCs contain only one labile hydrogen atom, thus, only single deuteration, formally forming an $[M + D]^+$ ion, was observed. With regard to all other features, the results obtained with the PC standard fully resemble those obtained with PS described above; regular MALDI-MS performed with deuterated

matrix yields $[PC(34:1) + D]^+$, while the engagement of PI leads to DHX and the formation of $[M + H]^+$. In a D_2O-enriched gas atmosphere, the PI step leads to the formation of intensive $[PC(34:1) + D]^+$ signals.

The degree of fragmentation reactions in MALDI and MALDI-SPICI may to first-order be assessed by the loss of the headgroup (HG; $C_3H_5O_2N$) from the PS standard (Fig. 5c1). The dominant fragmentation product $[M - HG - H + 2Na]^+$ is detected with a relative intensity of ~ 40% compared to the intact precursor – note that the relatively high degree of fragmentation, [9] in this case, is due to the high laser fluence, which in all standard measurements was set to the same value as used for the MALDI-SPICI experiments. Upon PI, solely the $[M + H]^+$ signal of the PS increases in intensity by about two orders of magnitude. (Fig. 5c2) and the $[M - HG + H]^+$ fragment is detected with only 10 % relative intensity compared to the intact $[M + H]^+$ species. Although at this stage, it cannot be fully excluded that some fragmentation may occur during the PI steps, the data suggest that the detected signals are mostly the result of the postionization of fragments generated in the initial MALDI event. Similar findings were reported for laser-based MALDI-2. [11]

The results from analogous experiments with the PC(16:0/18:1) standard are shown in Figure S-8 (SI). Also here, the PI process specifically enhanced the generation of protonated species, with only a minute degree of fragmentation.

Conclusions

In summary, we present the successful implementation of pulsed RF-Kr discharge lamps and volatile dopants for efficient PI of glycerophospho- and (glyco)sphingolipids and numerous further compounds in high-resolving MALDI-MS imaging. Particularly ‘soft and simple’ but effective ionization of laser-desorbed particles allows for the generation of mass spectra generally similar to laser-based MALDI-2. However, the secondary ionization pathways observed in our study reflect a different chemical interplay in the dense micro reaction environment and, therefore, can be described neither as a matrix-assisted nor as a direct SPI process. After excitation of acetone molecules through SPI, complex reaction cascades at distinct pressure conditions between analytes, dopant, and water in the plume lead to the formation of $[M + H]^+/[M - H]^-$ species with little to no fragmentation.

In comparison to laser-based MALDI-2, the developed SPICI module readily enables operation with kHz acquisition rates and could as well be operated in the continuous wave mode if combined with laser repetition rates exceeding 1 kHz and fast data acquisition mass spectrometers. [18] Moreover, our VUV lamp-based PI source is more cost-effective. An optimized ion source design may in the future help to reduce the high chemical background, which currently hampers analyses in the *m/z* range below about 450 Da in the positive ion mode. Furthermore, the use of different dopants, as well as matrix-free LDI techniques, could further broaden the range of analyte classes amenable to the method. All features together could render the presented MALDI-SPICI methodology a useful addition to the bioanalytical toolbox for mass spectrometry imaging.

Declarations

Acknowledgements

We thank Ansgar Korf (Bruker Daltonik) for assistance with MZmine 2 software, Sara Tortorella (Molecular Horizon) for providing LipostarMSI software, Willi Kramer (University Hospital Münster) for production of Figures 1 and S-1, Marcel Niehaus and Fabian Eiersbrock for assistance with the design process of the ion source and sample preparation, respectively, Jan Schwenzfeier for support with python scripts, and Alexander Potthoff, Gottfried Pohlentz, and Michael Mormann for numerous helpful discussions. Financial support by the German Research Foundation (DFG; grants DR416/12-1 and SO476/3-1, project number 290343045, and DR416/13-1 and SO476/4-1, project number 326945247; both to K.D. and J.S.) is gratefully acknowledged.

Author contributions

C.B., K.D., and J.S. conceived the experiments; C.B. and J.S. designed the VUV-based ion source; U.R. designed the class E amplifier to drive the VUV lamps; C.B., U.R., and J.S. adjusted the class E amplifier for pulsed use within the dual-ion funnel injector; C.B. conducted the experiments and performed the data analysis; C.B., K.D., and J.S. wrote the paper.

Competing interests

All authors declare no competing interests.

References

1. McDonnell, L. A. & Heeren, R. M. A. Imaging mass spectrometry. *Mass Spectrom. Rev.* **26** (4), 606–643 (2007).
2. Buchberger, A. R., DeLaney, K., Johnson, J. & Li, L. Mass Spectrometry Imaging: A Review of Emerging Advancements and Future Insights. *Chem.* **90** (1), 240–265 (2018).
3. Hanley, L., Wickramasinghe, R. & Yung, Y. P. Laser Desorption Combined with Laser Postionization for Mass Spectrometry. *Rev. Anal. Chem.* **12** (1), 225–245 (2019).
4. Ding, X., Liu, K. & Shi, Z. Laser desorption/ablation postionization mass spectrometry: recent progresses in bioanalytical applications. *Mass Spectrom. Rev.* **40** (4), 566-605 (2020).
5. Palmer, A., Trede, D. & Alexandrov, T. Where imaging mass spectrometry stands: Here are the numbers. *Metabolomics* **12** (6), 422 (2016).
6. Kompauer, M., Heiles, S. & Spengler, B. Atmospheric pressure MALDI mass spectrometry imaging of tissues and cells at 1.4-μm lateral resolution. *Methods* **14**, 90-96 (2017).

7. Niehaus, M., Soltwisch, J., Belov, M. E. & Dreisewerd, K. Transmission-mode MALDI-2 mass spectrometry imaging of cells and tissues at subcellular resolution. *Methods* **16** (9), 925–931 (2019).
8. Robinson, K. N., Steven, R. T., Race, A. M. & Bunch, J. The Influence of MS Imaging Parameters on UV-MALDI Desorption and Ion Yield. *Am. Soc. Mass Spectrom.* **30** (7), 1284–1293 (2019).
9. Schiller, J. *et al.* Matrix-assisted laser desorption and ionization time-of-flight (MALDI-TOF) mass spectrometry in lipid and phospholipid research. *Lipid Res.* **43**, 449–488 (2004).
10. Boskamp, M. S. & Soltwisch, J. Charge Distribution between Different Classes of Glycerophospolipids in MALDI-MS Imaging. *Chem.* **92** (7), 5222–5230 (2020).
11. Soltwisch, J. *et al*. Mass spectrometry imaging with laser-induced postionization. *Science* **348** (6231), 211–215 (2015).
12. Potthoff, A., Dreisewerd, K. & Soltwisch, J. Detailed Characterization of the Postionization Efficiencies in MALDI-2 as a Function of Relevant Input Parameters. *Am. Soc. Mass Spectrom.* **31** (9), 1844–1853 (2020).
13. Barré, F. P. Y. *et al*. Enhanced Sensitivity Using MALDI Imaging Coupled with Laser Postionization (MALDI-2) for Pharmaceutical Research. *Chem*. **91** (16), 10840–10848 (2019).
14. Bednařík, A., Bölsker, S., Soltwisch, J. & Dreisewerd, K. An On-Tissue Paternò-Büchi Reaction for Localization of Carbon-Carbon Double Bonds in Phospholipids and Glycolipids by Matrix-Assisted Laser-Desorption-Ionization Mass-Spectrometry Imaging. *Chem. Int. Ed.* **130** (37), 12268–12272 (2018).
15. Brockmann, E. U., Steil, D., Bauwens, A., Soltwisch, J. & Dreisewerd, K. Advanced Methods for MALDI-MS Imaging of the Chemical Communication in Microbial Communities. *Chem.* **91** (23), 15081–15089 (2019).
16. Bowman, A. P. *et al*. Evaluation of lipid coverage and high spatial resolution MALDI-imaging capabilities of oversampling combined with laser post-ionisation. *Bioanal. Chem.* **412** (10), 2277–2289 (2019).
17. Heijs, B., Potthoff, A., Soltwisch, J. & Dreisewerd, K. MALDI-2 for the Enhanced Analysis of N-Linked Glycans by Mass Spectrometry Imaging. *Chem.* **92** (20), 13904–13911 (2020).
18. Soltwisch, J. *et al*. MALDI-2 on a Trapped Ion Mobility Quadrupole Time-of-Flight Instrument for Rapid Mass Spectrometry Imaging and Ion Mobility Separation of Complex Lipid Profiles. *Chem.* **92** (13), 8697–8703 (2020).
19. Elia, E. A., Niehaus, M., Steven, R. T., Wolf, J.C. & Bunch, J. Atmospheric Pressure MALDI Mass Spectrometry Imaging Using In-Line Plasma Induced Postionization. *Chem.* **92** (23), 15285–15290 (2020).
20. Hanley, L. & Zimmermann, R. Light and molecular ions: the emergence of vacuum UV single-photon ionization in MS. *Chem.* **81** (11), 4174–4182 (2009).
21. Shi, Y. J. & Lipson, R. H. An overview of organic molecule soft ionization using vacuum ultraviolet laser radiation. *J. Chem.* **83** (11), 1891–1902 (2005).

22. Schätti, J. *et al.* Pushing the mass limit for intact launch and photoionization of large neutral biopolymers. *Commun Chem* **1**, 93 (2018).
23. Kauppila, T. J., Syage, J. A. & Benter, T. Recent developments in atmospheric pressure photoionization-mass spectrometry. *Mass Spectrom. Rev.* **36** (3), 423–449 (2017).
24. Syage, J. A., Hanning-Lee, M. A., & Hanold, K. A. A man-portable, photoionization time-of-flight mass spectrometer. *Field Analyt. Chem. Technol.* **4** (4), 204–215 (2000).
25. Bookmeyer, C., Soltwisch, J., Röhling, U. & Dreisewerd, K. Low-Pressure Photoionization in a Dual-Ion Funnel Injector Coupled to an Orbitrap Mass Spectrometer for Direct Analysis of Human Breath and Head-Space Sampled Coffee Roasts. *ChemPlusChem* **85** (7), 1559–1563 (2020).
26. Cui, Y. *et al.* Molecular Imaging and Depth Profiling of Biomaterials Interfaces by Femtosecond Laser Desorption Postionization Mass Spectrometry. *ACS Appl. Mater. Interfaces* **5** (19), 9269–9275 (2013).
27. Hsu, H. & Ni, C.-K. Vacuum Ultraviolet Single-Photon Postionization of Amino Acids. *Sci.* 8 (5), 699 (2018).
28. Fahy, E., Sud, M., Cotter, D. & Subramaniam, S. LIPID MAPS online tools for lipid research. *Nucleic Acids Res.* **35**, W606–W612 (2007).
29. Cífková, E., Holčapek, M. & Lísa, M. Nontargeted lipidomic characterization of porcine organs using hydrophilic interaction liquid chromatography and off-line two-dimensional liquid chromatography-electrospray ionization mass spectrometry. *Lipids* **48** (9), 915–928 (2013).
30. Choi, J. *et al.* Comprehensive analysis of phospholipids in the brain, heart, kidney, and liver: brain phospholipids are least enriched with polyunsaturated fatty acids. *Cell. Biochem.* **442** (1-2), 187–201 (2017).
31. Ellis, S. R. *et al*. Automated, parallel mass spectrometry imaging and structural identification of lipids. *Methods* **15** (7), 515–518 (2018).
32. Zhang, T., Chen, S., Liang, X., & Zhang, H. Development of a mass-spectrometry-based lipidomics platform for the profiling of phospholipids and sphingolipids in brain tissues. *Bioanal. Chem.* **407** (21), 6543–6555 (2015).
33. Ellis, S. R., Soltwisch, J., Paine, M. R. L., Dreisewerd, K. & Heeren, R. M. A. Laser post-ionisation combined with a high resolving power orbitrap mass spectrometer for enhanced MALDI-MS imaging of lipids. *Chemical Communications* **53**, 7246–7249 (2017).
34. Raddatz, C.-R., Allers, M., Kirk, A. T. & Zimmermann, S. Acetone and perdeuterated acetone in UV-IMS. *J. Ion Mobil. Spec.* **21** (3), 49–53 (2018).
35. Kostyukevich, Y. *et al.* Hydrogen/Deuterium Exchange Aiding Compound Identification for LC-MS and MALDI Imaging Lipidomics. *Chem.* **91** (21), 13465–13474 (2019).
36. Chambers, M. C. *et al*. A cross-platform toolkit for mass spectrometry and proteomics. *Biotechnol*. **30** (10), 918–920 (2012).

37. Goracci, L., *et al.* Lipostar, a Comprehensive Platform-Neutral Cheminformatics Tool for Lipidomics. *Chem*. **89** (11), 6257– 6264 (2017).
38. Pluskal, T., Castillo, S., Villar-Briones, A. & Oresic, M. MZmine 2: modular framework for processing, visualizing, and analyzing mass spectrometry-based molecular profile data. *BMC Bioinformatics* **11**, 395 (2010).
39. Korf, A., Jeck, V., Schmid, R., Helmer, P. O. & Hayen, H. Lipid Species Annotation at Double Bond Position Level with Custom Databases by Extension of the MZmine 2 Open-Source Software Package. *Anal. Chem.* **91** (8), 5098–5105 (2019).

Methods

Chemicals. Lipid standards 1-palmitoyl-2-oleoyl-sn-glycero-3-phospho-L-serine (sodium salt) (PS(16:0/18:1)) and 1-palmitoyl-2-oleoyl-sn-glycero-3-phospho-L-phosphocholin (sodium salt) (PC(16:0/18:1)) were from Avanti Polar Lipids (Alabaster, AL), deuterated methanol (MeOD; 99 % D) was from Acros Organics (Geel, Belgium). All other chemicals were purchased from Merck/Sigma-Aldrich (Steinheim, Germany).

Tissues. Mouse brain and kidney were dissected from 10–15-week-old female C57BL6/J mice, according to approved protocols. Whole organs were embedded in 2-hydroxyethylcellulose (M_{avg} ~1,500,000 g/mol) and then snap-frozen in liquid N_2. Pig brain was from a local butchery and bulk homogenate was prepared as described. [11] Briefly, brain tissue was snap-frozen in liquid N_2 and 7 g of homogenized tissue was mixed with 3 g of aqueous 2-hydroxyethylcellulose polymer solution. Tissue sections of 10 µm thickness (mouse) or 20 µm thickness (pig brain homogenate) were produced with a cryotome (Jung Frigocut 2800E, Leica Biosystems, Jena, Germany) and thaw-mounted on histological glass slides (SuperFrost, Fisher Scientific, Schwerte, Germany).

Lipid standards were prepared to 1 µmol/L in 70 % acetonitrile and evenly coated onto histological glass slides using an ultrasonic sprayer (SimCoat, Sono-Tek, Milton, NY). 400 µL of standard solution were sprayed at a flow rate of 0.03 mL/min in meandering patterns at a distance of 1.8 mm between the lines. Tissue sections and slides with standards were stored at −78 °C until further use.

Deuterated matrix was synthesized by dissolving 0.2 g of DHAP in 30 mL of a mixture of deuterated methanol (MeOD) and acetone-d_6 (50:50, v:v), followed by removing the solvents in a rotary evaporator (VV2011, Heidolph Instruments, Schwabach, Germany). To ensure a close to complete degree of deuterium exchange, the process was repeated three times so that in the later mass spectrometric analysis no protonated signal of the matrix was detected. The crystalline deuterated matrix was stored at -20 °C in a sealed glass flask until further use. During synthesis and storage, the deuterated matrix was kept under dry argon.

After removal from the freezer, tissue sections and standards were thawed under a stream of nitrogen before coating with the MALDI matrix in a home-build matrix sublimation chamber. [10] 1.2 mL of matrix solution (DHAP: 7 mg/mL in 70 % acetonitrile (ACN); *deuterated* DHAP: 7 mg/mL in MeOD/acetone-d_6 (50:50, v:v) were filled into the matrix reservoir of the sublimation chamber and the reservoir was heated to 135 °C. The sample slide was mounted onto a cooling socket at about 3.5 °C. The sublimation chamber was evacuated to approximately 10^{-4} mbar. To stop the sublimation process, the chamber was flushed with nitrogen. [10] MALDI samples were recrystallized for 2.5 min at 70 °C in an atmosphere containing 0.5 % ethanol in H_2O.

Mass spectrometer. A Q Exactive Plus Orbitrap (Thermo Fisher Scientific, Bremen, Germany), coupled with a dual-ion funnel/dual MALDI/ESI Injector (Spectroglyph, Kennewick, WA), was used as the mass analyzer. The ion source has previously been modified to enable laser-based MALDI-2. [7,14] A modified version was also used in our initial LPPI work with (s)VOCs. [25]

A frequency-tripled q-switched Nd:YLF laser (Explorer One, Spectra-Physics, Mountain View, CA; emission wavelength: 349 nm; pulse width: 7-10 ns; pulse repetition rate $f_{rep,}$ adjustable from 1 up to a maximum of 5 kHz) was used as the MALDI laser and for material ablation in the MALDI-SPICI experiments. In the presented spectra, the ablation laser was operated with a repetition rate of 300 Hz.

The default lens that is used in the Spectroglyph ion source to focus the laser beam on the target was replaced by two CaF_2 planoconvex lenses (Thorlabs, Dachau, Germany) with focal lengths of 300 mm and 1000 mm. By this replacement, the combined focal length of the optical system fits the requirements of the source more precisely and enables the production of an effective spot size of ~9 µm (defined as the area of visible material ejection).

To reduce background ion signal levels, throughout our experiments the ESI inlet of the MALDI/ESI Injector was blocked with a polytetrafluoroethylene (PTFE) plug. A fine-needle valve (SS-1RS6MM, 0.37 Cv, Swagelok, Düsseldorf, Germany) was used to adjust the N_2 buffer gas pressure in a range of 4-12 mbar in the region of the primary ion funnel. Optionally, dopant vapor from the headspace of a sealed reservoir flask was introduced into the ionization chamber via a PTFE tubing (outer diameter, 3/8”) and Swagelok® fittings. A second needle valve (SS-ORS3MM, 0.09 Cv, Swagelok, Düsseldorf, Germany) was used to manually control the gas flow of dopant into the funnel. For one experiment, another PTFE tubing connected a D_2O chamber with the ion source in a similar manner. The D_2O chamber contained a glass vial filled with D_2O. The chamber was evacuated, closed by another needle valve, and the vial was broken inside the closed chamber. The pure D_2O vapor was introduced at controlled amounts through the valve. The determination of the partial pressure of the introduced gases was based on an approximation by monitoring the Pirani pressure gauge of the Spectroglyph system.

During the experiments, three different mass resolving powers of the Orbitrap of Res_m = 70,000, 140,000, and 280,000 (each defined for an *m/z* value of 200) were used. The “injection time” was set to a fixed value of 250, 500, and 900 ms for the three resolution values, respectively, resulting in data acquisition rates of 3.7, 1.9, and 0.97 pixels per second. The “AGC target” was disabled.

For higher-collision induced dissociation (HCD) tandem MS measurements, the analytical quadrupole was set to an isolation window of 0.8 Da and the collision energy (CE) was varied between 12 and 30 eV (laboratory frame). For data-dependent acquisition (DDA) of a coronal brain section, the “dynamic exclusion” was set to 9 s (for brain homogenate to 45 s) and the ACG threshold to 2×10^4. An “exclusion list” was generated prior to each experimental run with background signals of a blank spectrum acquired at equilibrated measurement conditions.

VUV module. The principle layout of the VUV SPI module has been described in detail previously. [25] A schematic of the design with measures is plotted in Figure S-1, a condensed sketch in Figure 1. Briefly, three RF-Kr discharge lamps (model PKR-106-6-14, Heraeus Noblelight, Hanau, Germany) were integrated into a custom-designed annular mount made of PEEK. The small size of the cylindrically shaped lamps with outer dimensions of 6 × 14 mm (diameter × length) allowed for positioning the lamps with optimized geometries in order to minimize perturbation of the electrical field in the central part of the ion funnel device. The distance of the emission side of the lamps to the MALDI sample was about 1 mm and the distance to the central axis of the ion funnel was ~5 mm. Adhesive copper band served to contact the lamps. The position of the electric contacts on the three lamp bodies – especially the distance between the two electrodes – needed to be essentially similar for all lamps in order to obtain homogeneous response characteristics upon pulsed electric excitation. A symmetric ring electrode connected the front-end (emission side) of the lamps serving as ground for excitation and ion extraction. A custom-made class E amplifier [25] operated the lamps via the copper electrodes at the back-end with an alternating current (AC) of 13.560 MHz and a peak-to-peak voltage of 220 V. A metal-oxide–semiconductor field-effect transistor (MOSFET; model IXZ631DF18N50, IXYS, Milpitas, CA) was triggered by an RF generator (TG2000 DDS function generator 20 MHz, Aim TTi, Huntingdon, UK) and induced a resonance circuit, which operated the lamps. Importantly, all electronic components were mounted outside the vacuum to minimize the effect of stray fields on the ion funnel. A direct current (DC) power supply (BA-315, Bertan Associates Inc., Syosset, NY) was used to supply the symmetric ground electrode at the lamp’s front-end with a variable DC voltage of 300-500 V.

As an important modification to our previous setup, [25] the RF generator was gated by a rectangular wave function generated by the internal pulse generator of an oscilloscope (InfiniiVision DSOX3032A, 350 MHz, 4GSa/s; Keysight Technologies, Santa Rosa, CA). The repetition rate was variable between 10 to 5000 Hz. This enabled the generation of pulsed VUV light with electric pulse widths between 70 µs and the continuous wave (cw) mode without modification of the in-source hardware; the minimum pulse width was found to ignite the lamps. The function generator also served for synchronization of ablation and

VUV pulses with variable repetition rates up to 5 kHz; the latter corresponds to the maximum pulse repetition rate of the laser; we note, the VUV lamps themselves could be operated with a frequency up to the continuous wave mode. A custom-made delay generator served for adjusting the delay between the actively q-switched Nd:YLF laser and the VUV pulses.

Another key feature for achieving constant signal intensities is the symmetric design of the central ring electrode (see Figure S-1, SI for details), which connects the VUV lamp's tips. By applying a constant DC voltage to the part of the lamps facing the plume, the electrodynamic field of the ion funnel device is affected. With a controlled symmetric "offset" being added, reproducible ion trajectories can effectively be realized. Generally, the applied DC voltage U_{xtr} as well as the total gas pressure P_{total} should be kept as constant as possible to ensure controlled and reproducible ion trajectories and thus to avoid variations in the ion counts or ion profiles. As shown in Figure 1f, a slight variation of U_{xtr} and P_{total} has only little effect on the observed ion counts and thus the exact optimization of these values plays only a minor role in the successful MALDI-SPICI experiment.

Data analysis. Xcalibur (vs. 4.0, Thermo Fisher Scientific) was used for the initial data examination and optionally for off-line recalibration of mass spectra. MSI data sets were converted to imzML-files by using ProteoWizard software [36] and uploaded to LipostarMSI (vs. 1.1; Molecular Horizon, Bettona, Perugia, Italy) for further graphical analyses. [28] Throughout this work all full scan ion images are presented using the viridis false-color scheme. The mass traces in the full scans of the DDA images were visualized in the rainbow false-color scheme and extrapolated to a five-pixel wide block by manually copying the information of signal intensities from the full scan pixels to the subsequent four pixels in the MSI picture file. MS/MS data were automatically annotated in LipostarMSI based on the DB manager – a complementary tool to LipoStar used to generate tandem MS data lists based on proprietary fragmentation rules. [37] Data sets of brain homogenate were uploaded to MZmine 2 software [38] for signal annotation of aligned lists with the tool "lipid search" and the integrated theoretical database [39]. Lipid identification was furthermore conducted via the online classification system of LIPID MAPS® [28] and by comparison with literature data. [16,29-32] All assignments are based upon using a mass tolerance of 1.5 ppm for R = 280,000 and 2 ppm for the lower mass resolution settings and were in several cases further confirmed by DDA.

Statistics and reproducibility. We recorded multiple measurements of different sample sections in both positive and negative ion mode within a period of about 12 months and could achieve a high degree of reproducibility among the different measurements.

MS measurements from brain homogenate in both ion modes were conducted with at least three independently prepared samples, which were yielding comparable results; e.g. a relative standard

deviation (RSD) of ~20 % in the intensities of annotated signals between measurements within 6 months and an according RSD <3.5 % within one set of measurements. For MSI experiments from brain tissue, three tissue sections from three different animals were analyzed in the positive ion mode yielding comparable results. Kidney was taken from one animal, only. Thus, in this case, only technical replicates were produced, again however yielding very comparable results. Lipid annotation was performed from averaged mass spectra of at least 10,000 pixels of the respective tissue sample and processed further as described above.

Data availability. The data that support the findings of this study, in particular all MSI data as presented in the main text, are available to download in the vendor-neutral imzML format from ____*insert link*____ or from the corresponding author upon request.

Figures

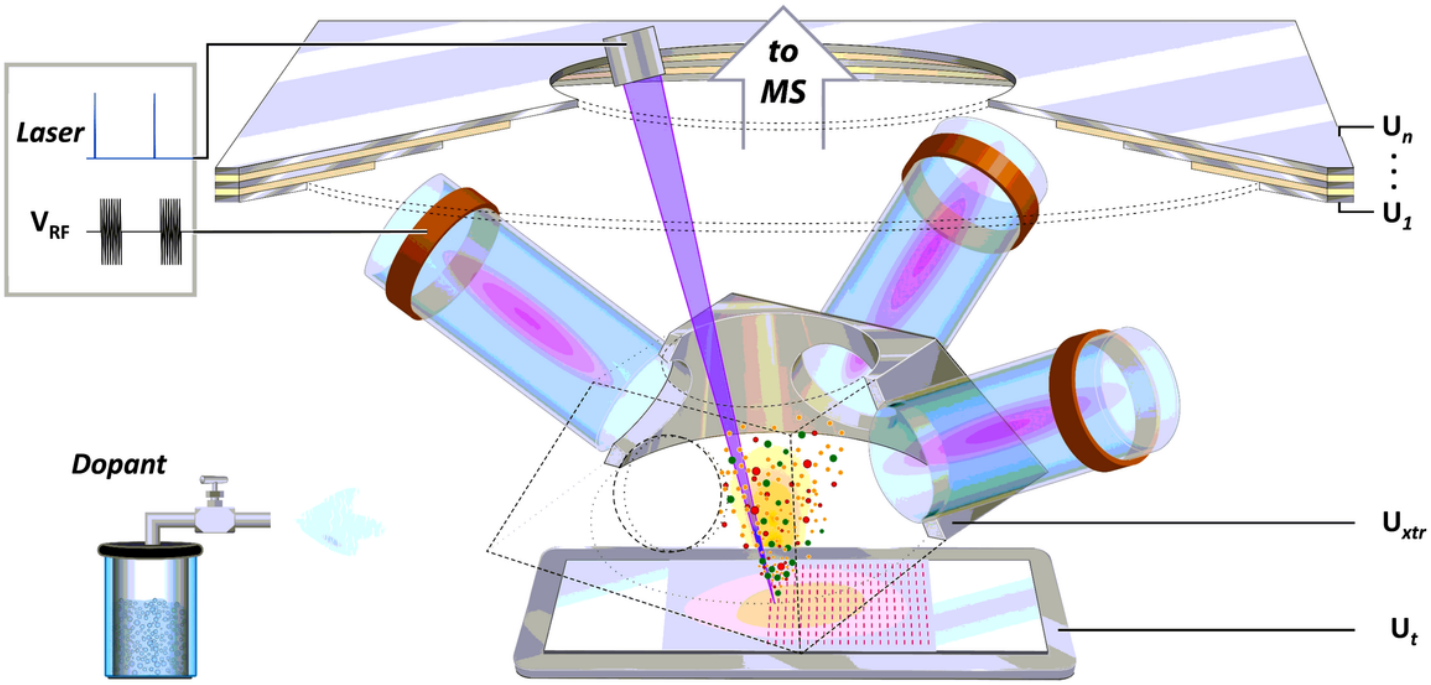

Figure 1

Schematic representation of the MALDI-SPICI ion source. Three symmetrically mounted Kr-discharge lamps are directed at an angle of 40° towards the particle plume generated by the pulsed MALDI laser from a matrix-coated sample. A symmetric ring electrode, supplied with an extraction voltage Uxtr enables undisturbed ion extraction between the MALDI target at Ut and the funnel electrodes at U1..n. A

custom-made class E amplifier drives the RF lamps at 13.560 MHz with VRF and enables pulsed operation for optimal synchronization with the MALDI laser.

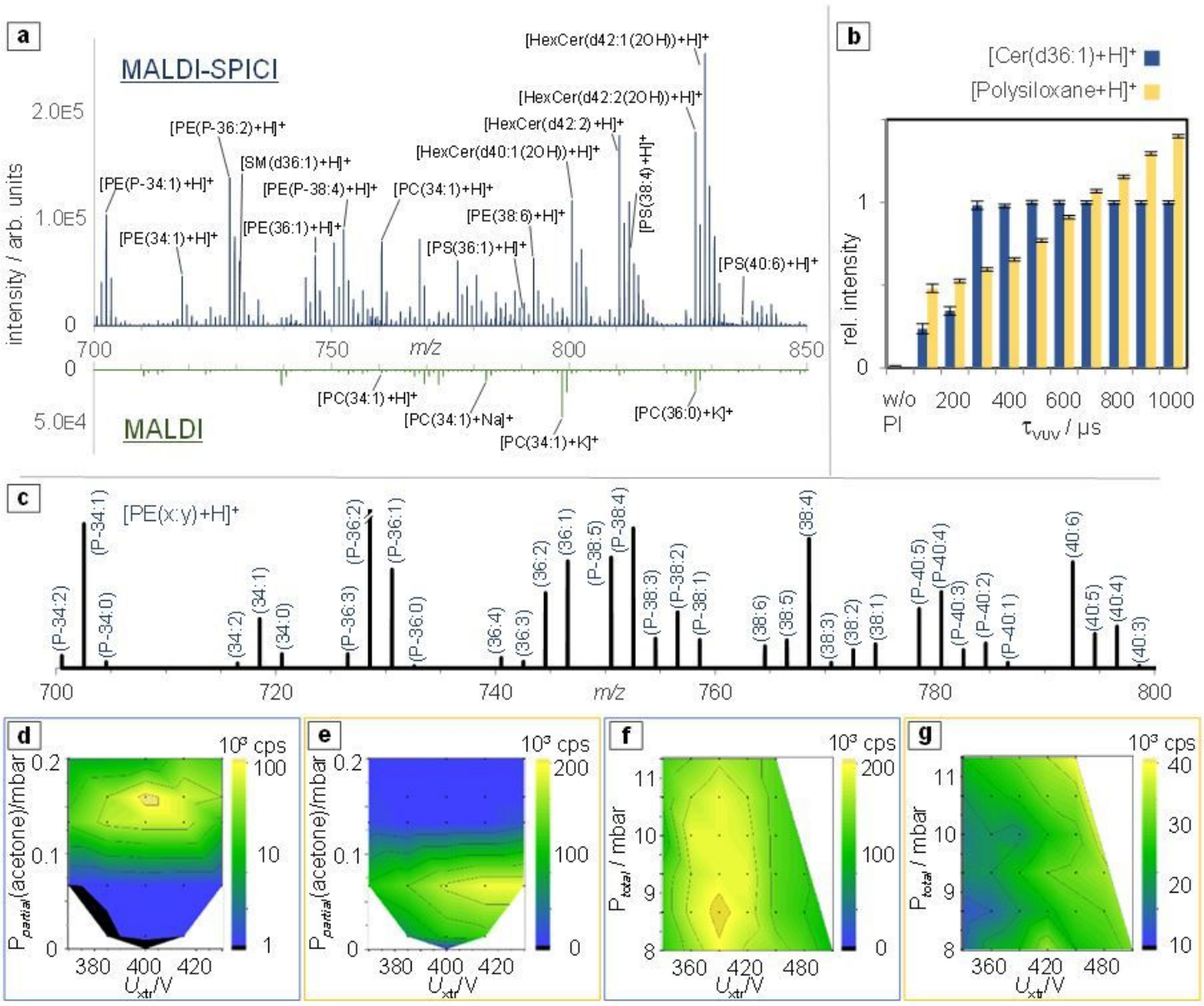

Figure 2

Parameter optimization. a: MALDI-SPICI (top) and MALDI-only (bottom) mass spectra of the central ‘phospholipid mass region’ between 700 and 850 Da. The mass spectra were recorded from a DHAP-coated section of pig brain homogenate; 300 pixels were summed in each case according to a total of 90,000 laser shots. b: Influence of the width of the VUV ignition pulse on the signal intensities of tentative [Cer(d36:1) + H]+ and on polysiloxane-derived background ion signals; c: Extracted [M + H]+ ion profiles for PE and PE plasmalogen species assigned based on accurate mass; exemplarily, only the plasmenyl variants are annotated. d,e: Heat maps showing the effect of the partial pressure of dopant (acetone) and Uxtr on the signal intensities of (d) tentative [Cer(d36:1) + H]+ and (e) polysiloxane background signals; f,g: Heat maps showing the effect of the total pressure and Uxtr for (f) tentative [Cer(d36:1) + H]+ and (g) polysiloxane background signals; black dots denote the experimental data points.

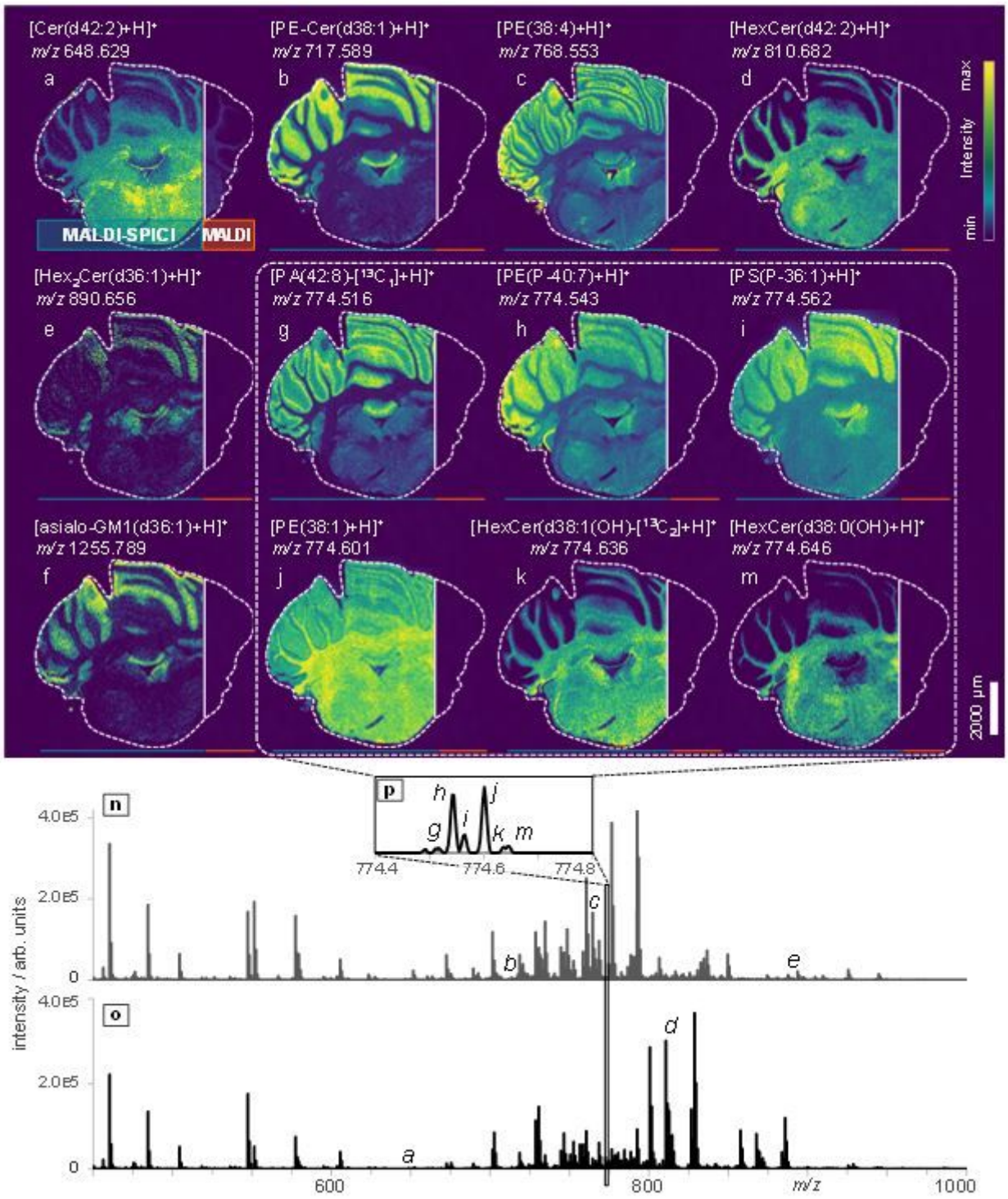

Figure 3

MALDI-SPICI-MS imaging of a coronal mouse brain section recorded in the positive ion mode. Upon MALDI-SPICI (left side of the images a-m), distinct distributions within the white and gray matter of the cerebellum and the medulla are obtained for numerous analytes, most of which are not detected with regular MALDI-MSI (right side). Data were recorded over 42 h at a pixel size of 16 µm and with frep = 300 Hz. Tentative assignments as denoted in the figure are based on accurate mass and literature data; n-o:

exemplary single-pixel MALDI-SPICI mass spectra recorded from (n) the molecular layer and (o) the white matter; p: zoom-in spectrum showing signals of 1000 averaged pixels in a 0.4 Da-wide window.

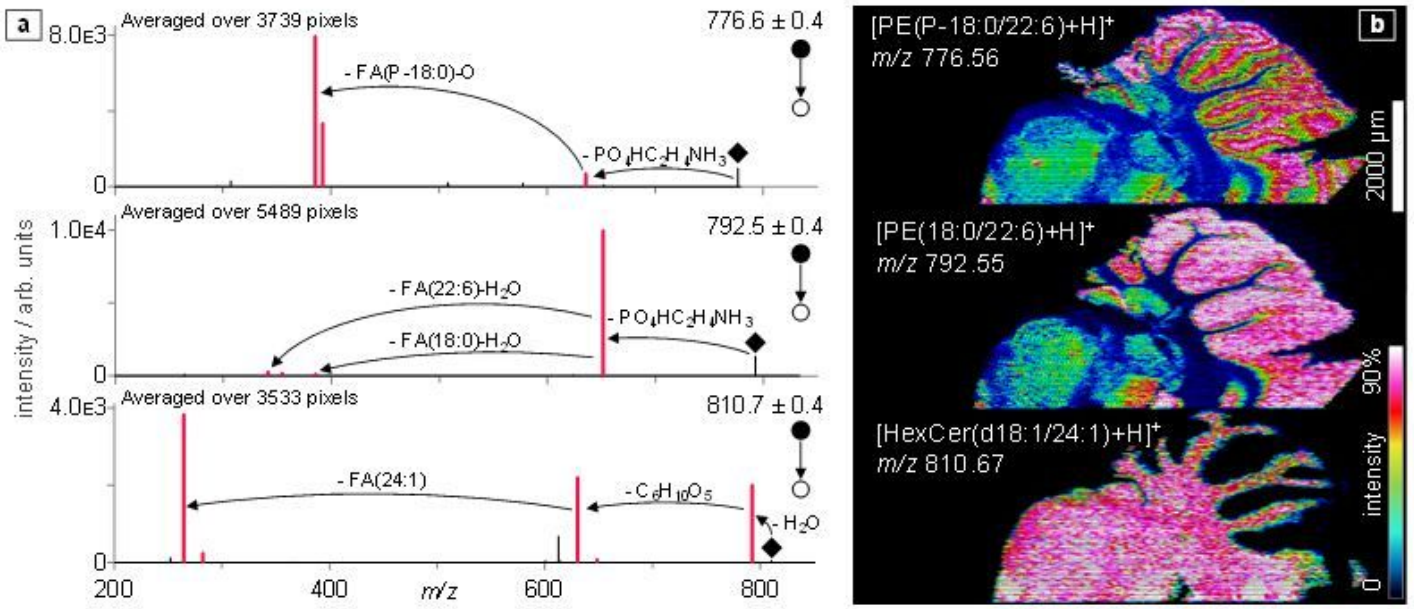

Figure 4

MALDI-SPICI-DDA-(MS/MS)-MSI of a mouse brain section. (a) Exemplary MS/MS spectra averaged over the indicated number of pixels; red signals represent fragments that confirm the annotated structure, ♦ mark the [M + H]+ precursor ions. (b) MSI signal intensity distribution of the identified lipids in the sequential full scans (extrapolated to a five-pixel wide block; see online methods). Data were recorded as a Top4-DDA experiment at a pixel size of 16 µm and frep = 300 Hz. The resolution for the full scan was Resm(MS1): 140,000 (defined for m/z 200; signal intensities not normalized) and for the tandem-MS was Resm(MS2): 70,000.

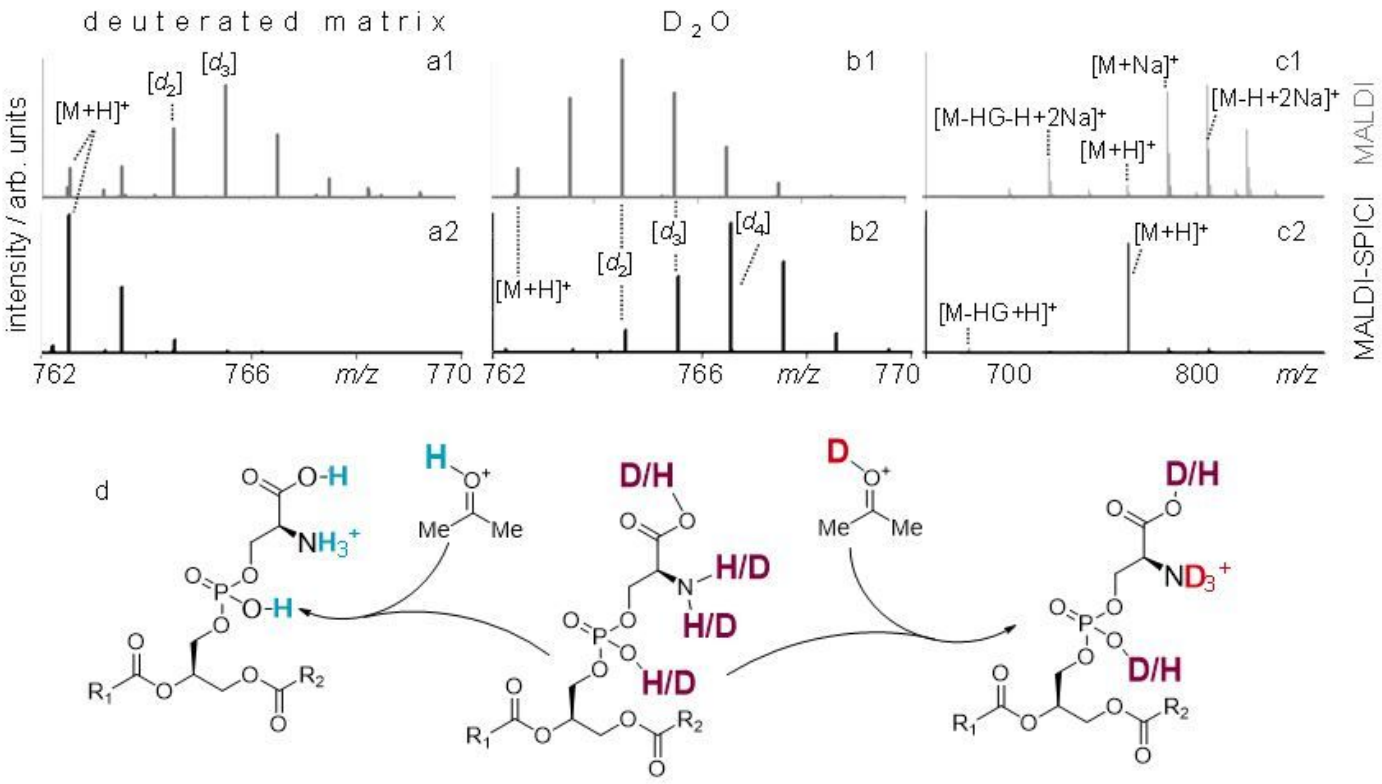

Figure 5

Deuteration and fragmentation experiments with PS(16:0/18:1) to reveal features of the ionization pathways. Mass spectra obtained with regular MALDI-MS and MALDI-SPICI-MS, respectively, show averages of 60 pixels. a1,a2: Zoom-in of mass spectra using the deuterated DHAP matrix; b1,b2: zoom-in of mass spectra using a D2O-enriched atmosphere; c1,c2: mass spectra without deuterated components; d: schematic suggested main gas-phase ionization step with protonated and deuteronated acetone, respectively. HG = head group (C3H5O2N), R1 = C(16:0), R2 = C(18:1) hydrocarbon chains.

Supplementary Files

This is a list of supplementary files associated with this preprint. Click to download.

- BookmeyeretalSupInfo.pdf
- SoltwischEPCFlats.pdf